

Spatial distribution of cloud droplets in a turbulent cloud-chamber flow

By A. JACZEWSKI¹* and S. P. MALINOWSKI²

¹*Institute of Meteorology and Water Management, Centre of Aerology, Legionowo, Poland*

²*Warsaw University, Institute of Geophysics, Poland*

(Received 4 May 2004; revised 4 January 2005)

SUMMARY

We present the results of a laboratory study of the spatial distribution of cloud droplets in a turbulent environment. An artificial, weakly turbulent cloud, consisting of droplets of diameter around $14\ \mu\text{m}$, is observed in a laboratory chamber. Droplets on a vertical cross-section through the cloud interior are imaged using laser sheet photography. Images are digitized and numerically processed in order to retrieve droplet positions in a vertical plane. The spatial distribution of droplets in the range of scales, l , from 4 to 80 mm is characterized by: the clustering index $CI(l)$, the volume averaged pair correlation function $\eta(l)$ and a local density defined on a basis of correlation analysis. The results indicate that, even in weak turbulence in the chamber that is less intense and less intermittent than turbulence observed in clouds, droplets are not spread according to the Poisson distribution. The importance of this deviation from the Poisson distribution is unclear when looking at $CI(l)$ and $\eta(l)$. The local density indicates that in small scales each droplet has, on average, more neighbours than expected from the average droplet concentration and gives a qualitative and intuitive measure of clustering.

KEYWORDS: Cloud microphysics Droplet distribution

1. INTRODUCTION

There are uncertainties concerning the existence of small-scale inhomogeneities in droplet spatial distribution resulting from small-scale turbulence in the unmixed volumes of clouds. Such inhomogeneities, if they exist, may influence the process of warm-rain formation (see reviews: Vaillancourt and Yau 2000; Shaw 2003) and affect radiative transfer through the clouds (see e.g. Kostinski 2001).

Evidence of non-random droplet distributions can be found in many reports. Baker (1992) reports a deviation from the Poisson distribution of droplets in segments on the scale of centimetres in convective cumulus clouds within regions that appear homogeneous on larger scales. Based on holographic measurements in fog (Kozikowska *et al.* 1984) and in stratiform orographic clouds (Uhlig *et al.* 1998) differences have been found between the observed spatial droplet distributions and random distributions. Kostinski and Shaw (2001) as well as Pinsky and Khain (2001, 2003), analysing aircraft data from the cores of cumulus clouds, report clustering of droplets on millimetre and centimetre scales. Other researchers (Brennguier 1993; Chaumat and Brennguier 2001), who investigated inter-droplet distances on one-dimensional horizontal cross-sections through the cores of cumulus clouds, provide experimental evidence that observed deviations from the Poisson distribution of cloud droplets are not statistically significant. It is evident, given this situation, that further research exploring the structure of small-scale atmospheric turbulence and its influence on droplet spacing is necessary.

Despite many efforts, complete *in situ* investigations of small-scale cloud structure are hardly practicable. Aircraft microphysical measurements with enhanced versions of the Forward Scattering Spectrometric Probes (FSSPs; e.g. Baumgardner *et al.* 1993; Brennguier 1993) suffer from too small a sampling volume. The FSSPs measure the positions of cloud particles along a one-dimensional section through the cloud, and a relatively long segment of the data (metres or more) has to be analysed in order to get a statistically significant result for the spatial distribution of droplets. Some of these

* Corresponding author: Institute of Geophysics, Pasteura 7, 02-093 Warszawa, Poland.

e-mail: malina@igf.fuw.edu.pl

© Royal Meteorological Society, 2005.

difficulties can be overcome by sophisticated data processing, where the assumption is made that the counting of droplets is a generalized Poisson process (Pawlowska *et al.* 1997). Moreover, there is no way to prove that the spatial distribution of droplets on such a long sample is governed mainly by the small-scale turbulence. Such processes as mixing of cloud parcels with different histories, and mixing with the dry environmental air are likely to be important. Studies concerning spatial distributions of droplets in a more isotropic, three-dimensional configuration (Kozikowska *et al.* 1984; Uhlig *et al.* 1998) are not subject to these limitations, but due to experimental difficulties only small datasets have been collected resulting in relatively large uncertainty in the results.

In the present paper we propose a new experimental approach to the problem, namely high-resolution observations of the droplet spatial distribution in a cloud generated in laboratory conditions. The intention is to simulate a homogeneous, well-mixed interior of the cloud, where droplet spatial distribution is influenced by small-scale turbulence. Laser sheet imagery—an experimental technique that we chose—allows for visualization of the cloud droplets in a two-dimensional, vertical, plane cross-section in the cloud interior. The experiment is designed to overcome the above mentioned drawbacks of *in situ* and holographic studies. Visualization of the chamber interior allows the exclusion of cases with mixing. The data collection technique adopted makes the statistical analysis highly reliable.

The laboratory cloud resembles a natural warm cloud in many aspects. It consists of water droplets whose sizes are similar to those observed in nature, while droplet velocities and positions are governed by small-scale turbulence. The most noteworthy difference between the chamber and real cloud interior is probably the turbulence itself; the motion in a chamber covers a much smaller range of spatial scales than in natural clouds. Possible effects of this difference are discussed later.

The paper is organized as follows. The description of the experiment, the details of the imaging and image-processing techniques are presented in section two. In the third section the statistical data analysis is described. The fourth section presents the results of the experiment, which are further discussed in section five. Conclusions are drawn in the last part of the paper.

2. LABORATORY EXPERIMENTS

(a) *Details of the experiment*

For the purpose of the present study we have modified the experimental system used by Malinowski *et al.* (1998, henceforward referred to as MZB) and Malinowski and Jaczewski (1999), in which the geometrical properties of an interface, separating cloudy and clear air filaments formed during turbulent mixing of a cloud with its environment, were investigated.

The core of the system is a cloud chamber of dimensions $1.8 \times 1 \times 1 \text{ m}^3$. A volume of saturated air carrying cloud droplets of diameters ranging from 7 to 25 μm enters the main chamber (Fig. 1). The droplets are generated by an ultrasonic droplet generator in a small chamber at the top of the experimental system. The central part of the cloud chamber is continuously illuminated by a 1.2 mm-wide sheet of light from an argon ion laser. The light, Mie-scattered at a 90° angle by cloud droplets, is imaged by a camera. The recorded images are then processed, digitized and analysed.

Modifications of the original MZB system have been introduced in order to improve its spatial resolution by:

(i) Increasing the power of the light source obtained by setting the laser to operate in multi-mode and therefore emitting light in 13 wavelengths. The two dominant spectral

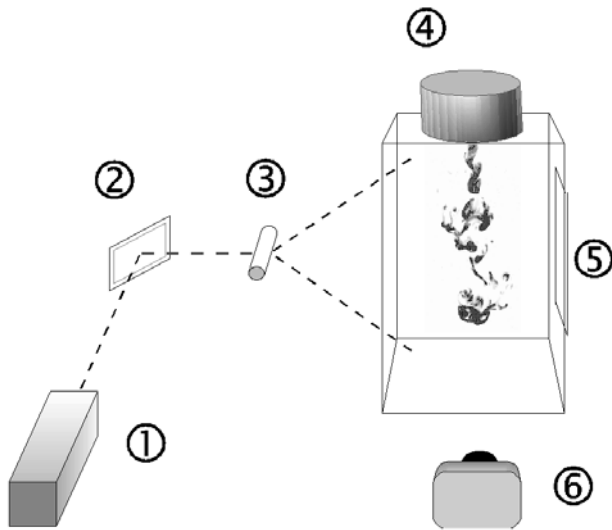


Figure 1. The experimental cloud-chamber set-up: (1) An argon ion laser (power = 3.5 W, 67% of the total beam output power at 488 nm and 514 nm wavelengths); (2) a mirror; (3) a cylindrical lens; (4) a small chamber with the droplet generator positioned inside; (5) the main chamber with a mirror; (6) a camera (panchromatic film forced to 6400 ASA, 135 mm lens).

lines, 514 nm green and 488 nm blue, make up approximately 67% of the total beam output power.

(ii) Adding a mirror at the wall of the chamber. The reflection almost doubles the light intensity in the imaging plane and, together with the multi-mode laser illumination, reduces the non-uniformity of the illuminating light.

(iii) Guiding the laser light into the chamber through a vertical aperture. In the earlier experiments laser light entered the chamber through a glass wall; the reflection then reduced the light intensity while diffraction induced non-uniformities of the light intensity in the sheet.

(iv) Increasing the camera lens aperture, and reducing the distance between the object plane and the lens plane. This enhances the amount of captured light, and increases the magnification, thus enhancing the spatial resolution and contrast.

As in the previous versions of the experiment (MZB) the photographic media used to capture images was Kodak T-MAX P3200 panchromatic film. However, during the chemical processing it was forced only to 6400 ASA sensitivity, not to 25000 ASA as before; this significantly reduced the grain size. The negative films obtained were digitized with 768 dots cm^{-1} (1950 dots per inch) resolution in 256 shades of grey.

The resulting size of a pixel was about $86 \times 86 \mu\text{m}^2$. Each pixel covered a volume 1.2 mm deep due to the thickness of the light sheet. The lens's depth of the field was about two times larger than this, so all illuminated droplets were imaged. The light sheet was located in the central part of the chamber. The camera's field of view covered a rectangle of 21 cm in the horizontal and 16 cm in the vertical, with the central point located 50 cm from the chamber walls in the middle of the light sheet.

In order to locate the moving droplets, the shutter speed had to be matched to the droplet velocities. Experience has shown that images obtained for relatively weak turbulent motions inside a cloud (decaying turbulence, with no dynamical forcing of the cloudy plume) with a shutter speed of $1/250 \text{ s}$ are sharp and possible to analyse. In these

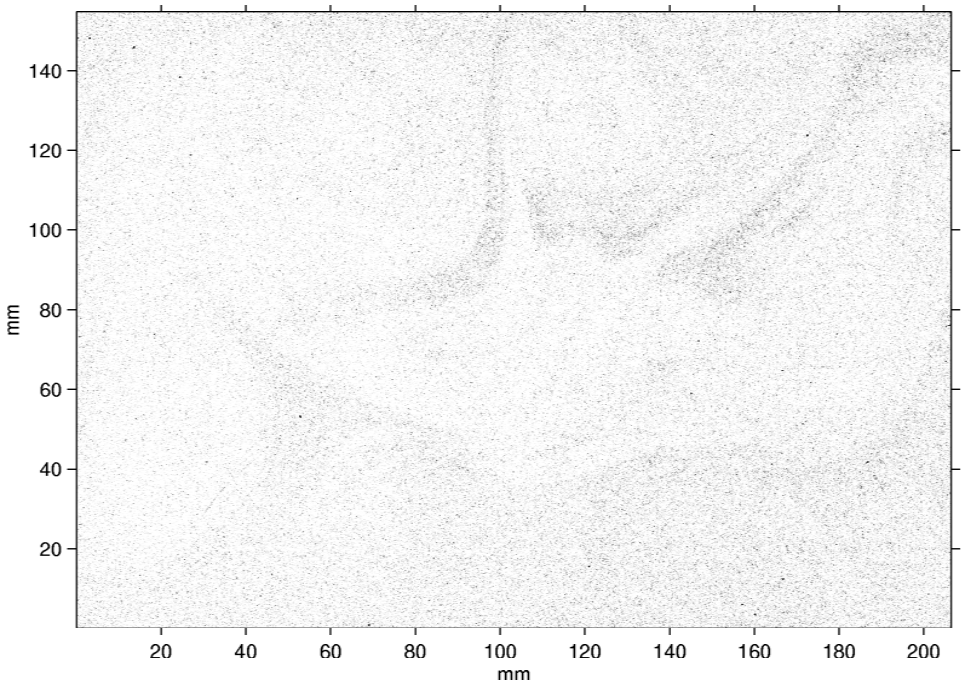


Figure 2. An example of an image of cloud droplets from the cloud-chamber experiment.

conditions the estimated droplet velocities due to turbulence and sedimentation usually do not exceed $\sim 3 \text{ cm s}^{-1}$. For the special case of droplets moving exactly in the plane of the image, the distance travelled by these droplets is $120 \mu\text{m}$ and may cover at the most three neighbouring pixels. The algorithm of automatic droplet detection in the image, described later, selects the brightest pixel only, i.e. light from an individual droplet is identified with one pixel of the digitized image.

In order to exclude non-uniform cloud (clear air filaments) due to inhomogeneous mixing with the environment, the whole observation chamber had to be filled with the cloud. After filling the main chamber, the inflow from the device containing the droplet generator was switched off. There was no external forcing of turbulence inside the chamber; it resulted from the initial mechanical production when filling the main chamber with cloud and from evaporative cooling of cloud droplets into the clear air inside the chamber during filling. Visual inspections of the chamber were performed in order to verify that all initial non-uniformities had disappeared due to mixing. Then, after 2–3 minutes, a series of 2–3 photographs were taken at about 30 s intervals. At such temporal intervals and turbulent velocities each image can be regarded as an individual scene, uncorrelated with preceding or later ones.

From more than 500 collected photographs, only a few tens were of high enough quality to digitize them with the resolution of 2400×1800 pixels. An inspection of the images reveals that the droplets form visible patterns (Fig. 2) qualitatively resembling those modelled by Vaillancourt *et al.* (2002). The final selection of images was carried out using photo-editing software. All scenes containing scratches, dust and other artefacts were discarded. After this procedure only ten of all the digitized images were finally selected for further processing.

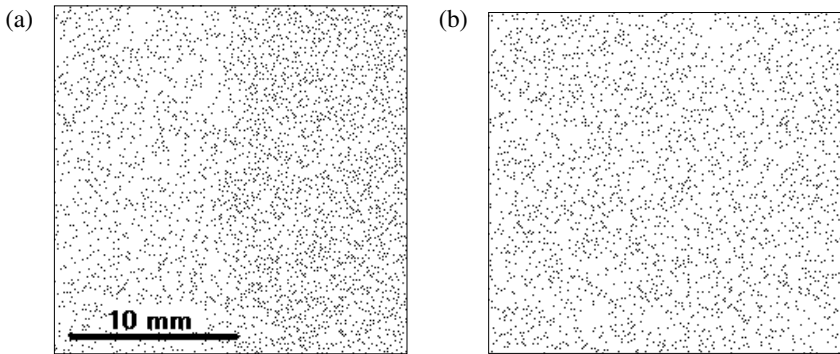


Figure 3. The droplet positions on: (a) a small segment of an example image from the cloud-chamber experiment, and (b) a similar segment of the artificially generated Poisson test image. The segment in (a) reveals a visible difference in droplet spacing between the left-hand and the right-hand parts of the image. This particular pattern was seen clearly over the whole image, and is presumably the effect of an inflow from the right-hand side of the image diverging in both directions along the line normal to the image plane.

At this stage, the position of each individual droplet in the scan was detected. The adopted algorithm selected pixels brighter than the four nearest neighbours in the principal directions of the image, thereby finding the local maxima in the image brightness. As a result of this simple procedure, pixels corresponding to the physical volume containing at least one droplet were marked black, and all others were marked white, forming a binary matrix representing droplet position in the planar section through the investigated volume of cloudy air. An example result of this procedure is presented in Fig. 3(a).

Finally, in order to verify that possible circulations on the scale of the whole chamber do not influence the droplet concentration on the scale of the image, each scene was divided in half in the horizontal and the vertical, and the mean concentrations of droplets in each half and also each quarter of the image calculated. No statistically significant differences in concentrations were detected.

(b) *Comparison of cloud chamber and natural cloud conditions*

A warm cloud, natural or artificial, consists only of water droplets and moist air surrounding them. Such a cloud can be characterized by droplet concentration, droplet size spectrum, liquid-water content etc. The thermodynamical properties of the air between droplets are described by temperature, pressure, and humidity. The dynamical properties of air depend on turbulence, e.g. on the turbulent energy dissipation rate, intermittencies, etc. The interactions between the droplets and the surrounding air are characterized by hydrodynamic interactions and droplet evaporation. In the following we briefly discuss possible similarities and differences between a natural cloud and the artificial cloud investigated here.

The temperature in the chamber during the experiment was 23–24 °C, slightly higher than in a typical low-level summer or tropical cloud. The initial relative humidity in the empty chamber was measured by psychrometer, and was in the range 65–70% for all the experiments. During imaging the air was saturated, its pressure was simply the atmospheric pressure, always close to 1000 hPa. Thus, the thermodynamic conditions in the chamber were not far from those in typical warm summer boundary-layer clouds.

The initial droplet spectrum was analysed in MZB. The mean droplet diameter of $14.9 \pm 5.5 \mu\text{m}$ is similar to many observations in real clouds, but concentrations

TABLE 1. MEAN DROPLET CONCENTRATIONS AND LOCAL DROPLET CONCENTRATIONS AT SCALES OF 4 AND 80 MM

Image number	Local droplet concentration at 4 mm scale (mm^{-2})	Mean droplet concentration (mm^{-2})	Local droplet concentration at 80 mm scale (mm^{-2})	$D - E$
Test	7.2	7.2	7.2	0.0001
1	7.5	7.1	6.8	-0.0346
2	9.1	8.7	8.6	-0.0236
3	9.4	9.0	8.8	-0.0245
4	8.9	8.6	8.5	-0.0150
5	9.7	9.4	9.5	-0.0093
6	7.7	7.3	7.2	-0.0193
7	9.3	9.1	9.0	-0.0122
8	6.3	6.2	6.1	-0.0080
9	5.4	5.3	5.2	-0.0108
10	5.5	5.3	5.2	-0.0169

Values are calculated according to (6) and the values of $D - E$ for the test image and for ten experimental images, where D is the correlation dimension and E is the Euclidean dimension. See text for details.

(4–9 mm^{-3}) are much higher than usually observed in nature. The droplets, however, are still relatively ‘rare’ in space (they occupy a small fraction of the volume). Since the observations do not cover the long-term evolution of the system, the interactions (possible collisions) of droplets should only affect droplet patterns to a small degree. On the other hand, such a high concentration enables good quality statistics of the investigated data to be obtained.

It is possible that droplets visualized in the images are slightly smaller than those measured in the initial spectrum, due to evaporation during the process of filling the chamber. This should, however, be a weak effect. An analysis performed in the numerical simulations of Andrejczuk *et al.* (2004), in conditions comparable to those in the chamber used here, showed a reduction of the mean diameter of droplets of not more than 10%.

An effort was made to collect images in comparable conditions: i.e. with the same temperature of the environment, and the same temperature and saturation of the cloudy air. The final liquid-water content in the chamber was not fully controlled but varied from one series to another, resulting in a remarkable variability of the observed droplet number concentration (Table 1).

The initial turbulent kinetic energy (TKE) dissipation rate inside the chamber, $\varepsilon = 6 \times 10^{-5} \text{ m}^2 \text{ s}^{-3}$ (MZB), is estimated from the velocity of the cloudy plume entering the main chamber and the size of the opening. This value suggests that small-scale turbulence in the chamber is less vigorous than that in real clouds (see e.g. Jonas 1996; Pinsky and Khain 2003). It should be noted, however, that the estimation method does not account for a significant source of TKE within the chamber, i.e. droplet evaporation. Results of numerical simulations by Andrejczuk *et al.* (2004) indicate that production of TKE by evaporative cooling of the cloudy plume when filling the chamber at the beginning of the experiment, substantially intensifies the small-scale turbulence. After 20 s of the simulations, when homogenization is almost complete, the Taylor microscale Reynolds number Re_λ is about 80 for small, moderate, and large initial TKE input from large scales. At this time the TKE level is comparable in all three cases after 20 s of simulations, and then slowly decays due to dissipation. Taking this into account, and knowing that the volume of the chamber is much larger than the volume of numerical experiment by Andrejczuk *et al.*, we expect that the intensity of the small-scale turbulence in the chamber during imaging is comparable to that from

the initial estimate. In this case the Stokes number for the typical droplet of $14 \mu\text{m}$ diameter is 0.006, and for the large droplet of $20 \mu\text{m}$ is 0.012. These values are small, suggesting that turbulence may influence droplet spatial distribution only marginally. In the following we show that even this marginal influence leads to a measurable clustering effect.

An important difference between the turbulence in the chamber and in real clouds is that the former allows a much smaller range of scales. Consequently, it is characterized by much smaller Reynolds number, $Re \sim 10^3$, than that attributed to turbulence in real clouds ($Re \sim 10^7$ to 10^9). Since the small-scale intermittency increases with Re (see e.g. Sreenivasan and Antonia 1997) there was little chance to observe any intensive small-scale vortices, characteristic of highly intermittent flows. Such vortices may strongly influence the distribution of cloud droplets (Bajer *et al.* 2000). On the other hand, such vortices are events with a very high TKE dissipation rate, and probably occupy only a small fraction of the volume of a real cloud (Grabowski and Vaillancourt 1999; Jeffery, 2001). Thus, the conditions in the chamber should resemble those in uniform volumes of clouds remote from such intermittent strong vortices.

Summarizing, we conclude that conditions in the chamber can be regarded as a satisfactory laboratory surrogate of a weakly turbulent real cloud. The major differences between a real cloud and the experiment are the more densely concentrated droplets, and weaker and less intermittent turbulence in the latter.

3. DATA ANALYSIS

Many aspects of the statistical analysis of the droplet spacing in clouds have been presented by Shaw *et al.* (2002). In the following, only a short description of the adopted methods is given; an exception is a correlation approach which is discussed in more detail in order to highlight different aspects from those in Shaw *et al.* (2002).

(a) Poisson approach

Let the random variable, N , represent a number of particles (droplets) in a sample of a given volume. The volume will be an interval of given length in the case of one-dimensional data (e.g. from the FSSP), a square fragment of our planar image, or a cubic segment of the investigated volume in the case of three-dimensional (e.g. holographic) data. Then, the mean \bar{N} and the variance $(\delta N)^2$ over all sampled volumes are computed. For the Poisson distribution of droplets inside non-overlapping samples the variance of counts equals the mean. This leads to the definition of CI , the clustering index:

$$CI = \frac{\overline{(\delta N)^2}}{\bar{N}} - 1, \quad (1)$$

which is zero for the Poisson droplet distribution in the investigated independent volumes.

In order to investigate dependence of the CI on the spatial scale, the space (image) is divided into segments ('hypercubes') of size l and volume l^E , where E is the Euclidean dimension of the sample ($E = 1$ for FSSP data, $E = 2$ for our case of planar image and $E = 3$ for the volumetric visualization of droplets in holographic experiments). The procedure is repeated for different l , resulting in a function $CI(l)$:

$$CI(l) = \{\overline{(\delta N_l)^2} / \bar{N}_l\} - 1. \quad (2)$$

Similar measures, sometimes slightly modified (the so-called Fishing test) were adopted by Baker (1992), Chaumat and Brenguier (2001) and Kostinski and Shaw (2001) in order to investigate FSSP data from real clouds.

Kostinski and Shaw (2001) show that $CI(l)$ must be interpreted with care, because its value at a given scale contains contributions from all smaller scales. Instead of CI , they suggest using the volume-averaged pair correlation function, which can be written as:

$$\eta(l) = CI(l)/\overline{N}_l. \quad (3)$$

It needs to be emphasized that information contained in $CI(l)$ and $\eta(l)$ as specified by (2) and (3) is exactly the same. It should also be pointed out that (3) was obtained assuming the form of the pair correlation function used in statistical physics (the gas equation, see Landau and Lifshitz 1980) with the additional assumption that $\overline{N}_l \sim CI^E$. Here C is the scale-independent, constant, hypervolume-averaged droplet concentration. It turns out that the difference between (2) and (3) comes from the division by a volume of a hypercube l^E , and (3) can be interpreted as proportional to the density of the clustering index. The importance and the meaning of this difference is discussed by Shaw *et al.* (2002).

(b) Correlation approach

Another type of analysis, sometimes called cluster or correlation analysis, is widely used in the fractal approach (see e.g. Feder 1988; Falconer 1990). Its principle is simple: for every point j of the analysed set (in our case every droplet in the image), the number k_{jr} of neighbours inside a ‘hyperball’ (circle in our case) of radius r centred on that point is computed, and averaged over all points. The result of this operation, when the set consists of N points is denoted as $\langle N \rangle_r$, and is interpreted as a mean number of droplets in a neighbourhood of size r around a typical droplet:

$$\langle N \rangle_r = \frac{1}{N} \sum_{j=1}^N k_{jr}. \quad (4)$$

Note the difference in averaging. In the previous subsection the mean was taken over independent, non-overlapping hypercubes (squares in the case of planar images). This was denoted by overbars, and in the following we refer to it as ‘volume averaging’. In this subsection we average over the overlapping neighbourhoods of individual droplets, i.e. over hyperballs centred around each droplet (circles in our case). This is denoted by square brackets and will be called ‘local averaging’. Different averaging leads to a different formulation of the problem of droplet clustering. The volume average is taken when we want to know how many droplets occupy a typical hypercube; the local average is taken when we want to know how many neighbours an average droplet has in its neighbourhood (hyperball) of a given radius. In fact, local averaging gives more information on the different statistics than volume averaging: i.e. correlations between the points of the set. When droplet positions are correlated, then the number of neighbours is different from that expected from the uncorrelated distribution.

The common approach is to investigate scaling properties of (4), i.e. to check whether:

$$\langle N \rangle_r \sim r^D \quad (5)$$

is fulfilled for a certain range of scales r . If so, then D is the correlation dimension valid in this range of scales (see e.g. Falconer 1990). A span of possible values of D is bounded from below by 0 and from above by the Euclidean dimension of the space

E in which the dataset is embedded (again $E = 1$ for one-dimensional data from the FSSP, $E = 2$ for dots in the two-dimensional planar image and $E = 3$ for positions in a three-dimensional space).

Note, that (4) can be reinterpreted in terms of a local mean droplet concentration $\langle C \rangle_r$:

$$\langle C \rangle_r = \frac{\langle N \rangle_r}{\alpha r^E}, \quad (6)$$

where $\alpha = 1$ for the one-dimensional data, $\alpha = \pi$ for two-dimensional data, and $\alpha = 4/3\pi$ for three-dimensional data; e.g. for the planar image ($E = 2$) (6) takes the form:

$$\langle C \rangle_r = \frac{\langle N \rangle_r}{\pi r^2}, \quad (7)$$

and $\langle C \rangle_r$ is understood as a mean local planar droplet concentration. When (5) is fulfilled, the above can be rewritten, and for a planar image we obtain :

$$\langle C \rangle_r \sim r^{D-2}. \quad (8)$$

and in the general case of E -dimensional space

$$\langle C \rangle_r \sim r^{D-E}. \quad (9)$$

For a random uncorrelated droplet distribution $\langle N \rangle_r \sim r^E$, which means that $\langle C \rangle_r = \text{constant}$, i.e. the mean local droplet concentration is independent of scale and is equal to the mean concentration C . When (5), and consequently (9), is fulfilled, then the exponent in D has to be smaller than the Euclidean dimension of the space. Generally, $\langle N \rangle_r$ does not need to scale according to (5); nevertheless $\langle C \rangle_r$ calculated according to (6) or (7) still contains information about mean local concentration.

It is worth mentioning, that (3) and (4)–(9) are based on the same mathematical foundation. Both can be derived from a pair correlation function, widely used in physics to describe the probability that two particles occupy the same location in space. The derivation (see Landau and Lifshitz 1980; Shaw *et al.* 2002) employs additional volume averaging and leads to (3). The derivation presented in Meakin (1998) uses local averaging and averaging over all directions only, and gives (4)–(9). Note also, that another very sophisticated analysis of droplet spatial correlations has been proposed by Pinsky and Khain (2001, 2003). Our data cover too small a range of scales to treat them with such an approach.

In practice, local averaging has to be performed carefully in order to avoid an artificial ‘edge effect’. In the local averaging, points located closer to the edge of a set than r are rejected (Fig. 4). Keeping them would artificially dilute the local concentration. This limits the range of scales investigated, because with increasing r the size of the sample decreases resulting in less reliable statistics.

4. RESULTS

The visual inspection of all collected images, as well as direct observations of the experiment in the cloud chamber, indicate the presence of patterns clearly seen with a sheet of light (Fig. 2). These patterns, evolving and appearing in a chamber even 30 minutes from the homogenization, take the form of spirals or rings, or at other times the form of ramps, comas or irregular elongated structures. Whether those patterns are created by the mechanisms proposed by Shaw *et al.* (1998) or Bajer *et al.* (2000) is still

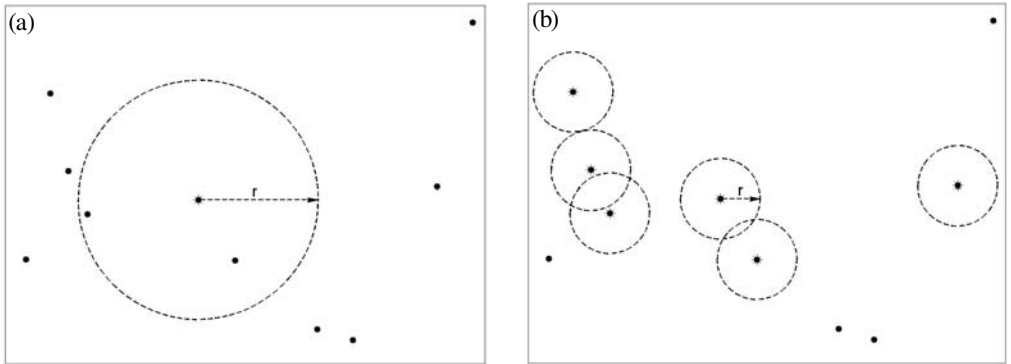


Figure 4. The principle of calculating $\langle N \rangle_r$, the mean number of droplets in a neighbourhood of size r around a typical droplet. In (a) only one droplet is far enough (distance greater than r) from the edge of the image, and $\langle N \rangle_r$ is computed only for that droplet. For smaller r , as shown in (b), there are more droplets fulfilling the criteria.

an open question. It seems, however, that even weak turbulent motion may influence the concentration of droplets at small scales.

In order to quantify the significance of this finding, all ten experimental images were analysed according to formulae (2), (3), (7) and (8). In order to test the computer codes and to compare the obtained results to a well-defined case, a special reference image with particles distributed according to the Poisson random distribution was artificially generated and analysed together with the experimental data. The average droplet concentration for this image was equal to the typical average concentration on experimental images (about 250 000 droplets per image). A segment of this is shown in Fig. 3(b).

In Fig. 5 a functional dependence of the clustering index $CI(l)$ on scale (box size) is plotted on a logarithmic axis. The thin solid line corresponds to the reference test image, while the results from the ten experimental images are marked by geometrical symbols. In all subsequent figures this same convention is adopted. The difference between the experimental data and the reference image is obvious in the range of scales above 5 mm and striking at scales above 20 mm. Worth noticing is the large spread of experimental results in different scenarios.

In Fig. 6, $\eta(l)$ is plotted. According to the discussion of (3), $\eta(l)$ can be understood as planar density of the clustering index. This leads to another interpretation of the experimental data; differences between results and the reference image are clear in the whole range of scales. The $\eta(l)$ peaks at around 2.5–3.4 mm, depending on the image, suggest preferential concentration at this scale. Deviations of the experimental data from the ideal Poisson process are evident. Again, while the shape of curves is similar for all the images investigated, the positions differ.

Data collected with the FSSP in real clouds, analysed by Kostinski and Shaw (2001), exhibit similar behaviour of $CI(l)$ and $\eta(l)$.

At this point we conclude that the experimental data differ from the ideal Poisson distribution. The interpretation of this deviation and understanding its significance is not intuitive. In the following section an interpretation of the same data in terms of (7) is seen to appear simpler and more convincing.

In Fig. 7 the dependence of local droplet concentration $\langle C \rangle_r$ on the scale $2r$ (circle diameter $2r$, to be compared with the box size l) is plotted for all ten images acquired in the experiment. The comparison of $\langle C \rangle_r$ in the reference image and in one of the

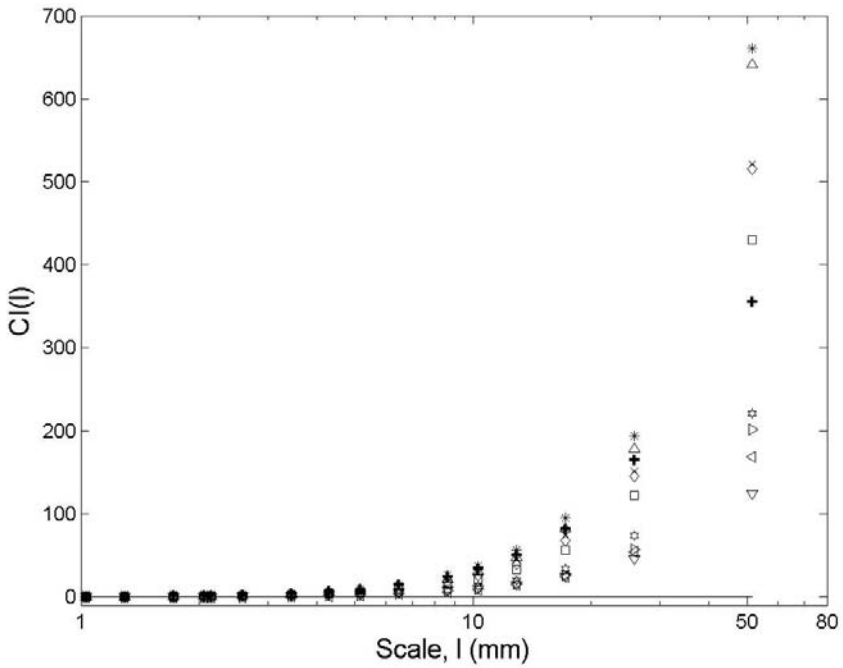


Figure 5. The dependence, calculated according to (2), of clustering index, $CI(l)$, on scale l for the artificially generated Poisson test image (continuous line) and for experimental images as shown individually by different symbols. See text for details.

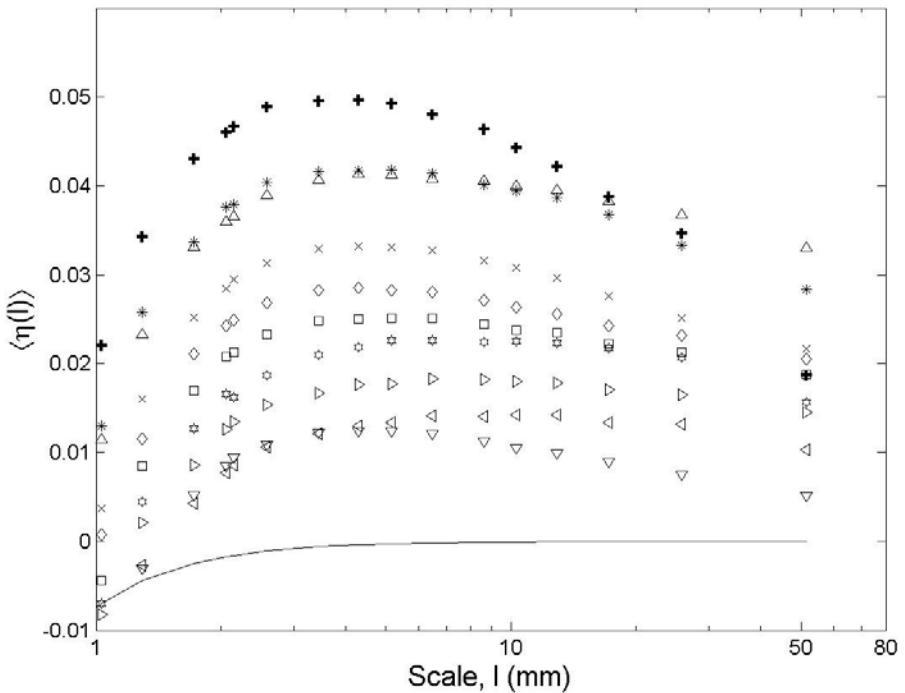


Figure 6. The dependence, calculated according to (3), of the volume averaged pair correlation function, $\eta(l)$, on scale l for the artificially generated Poisson test image (continuous line) and for the experimental images as shown individually by different symbols. See text for details.

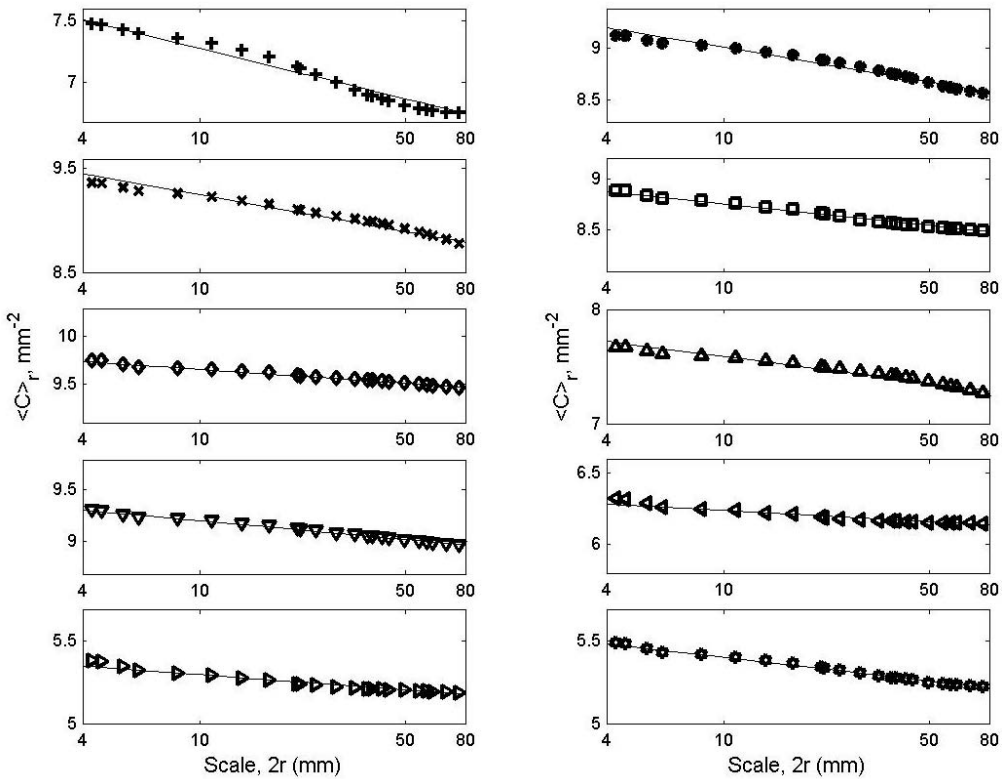


Figure 7. The dependence, calculated according to (7), of the local droplet concentration $\langle C \rangle_r$ on scale for each of the ten experimental images. See text for details.

experimental images is plotted in Fig. 8. In both Figs. 7 and 8 the scale on the vertical axis is logarithmic, i.e. the data are plotted in log–log coordinates. In this representation all images exhibit a gradual decrease in concentration with $2r$, in the range of scales from 4 to 80 mm. This means that the concentration of close neighbours of an average droplet is larger than the concentration of its far neighbours. In the analysed images and range of scales this difference is of the order of 3–10%. The local and mean droplet concentrations from all experimental images are given in Table 1.

The preferred scale, around 3.5 mm, suggested by the analysis of $\eta(l)$ in Fig. 6 cannot be excluded from the correlation analysis method, despite the fact that in scales smaller than 4 mm (not plotted here) we observe even higher local densities. This, however, can be an artefact of finite image resolution. On the other hand, Pinsky and Khain (2001, 2003) report that droplet correlations in smaller scales are becoming stronger. More measurements with better spatial resolution are necessary to investigate the spacing of droplets at scales smaller than 4 mm using the local concentration method.

The results plotted in Fig. 8 indicate that the experimental data have different characteristics from the reference set. In the reference Poisson image $\langle C \rangle_r$ is constant and equal to the mean concentration of droplets calculated as a ratio of the total number of droplets to the area of the image.

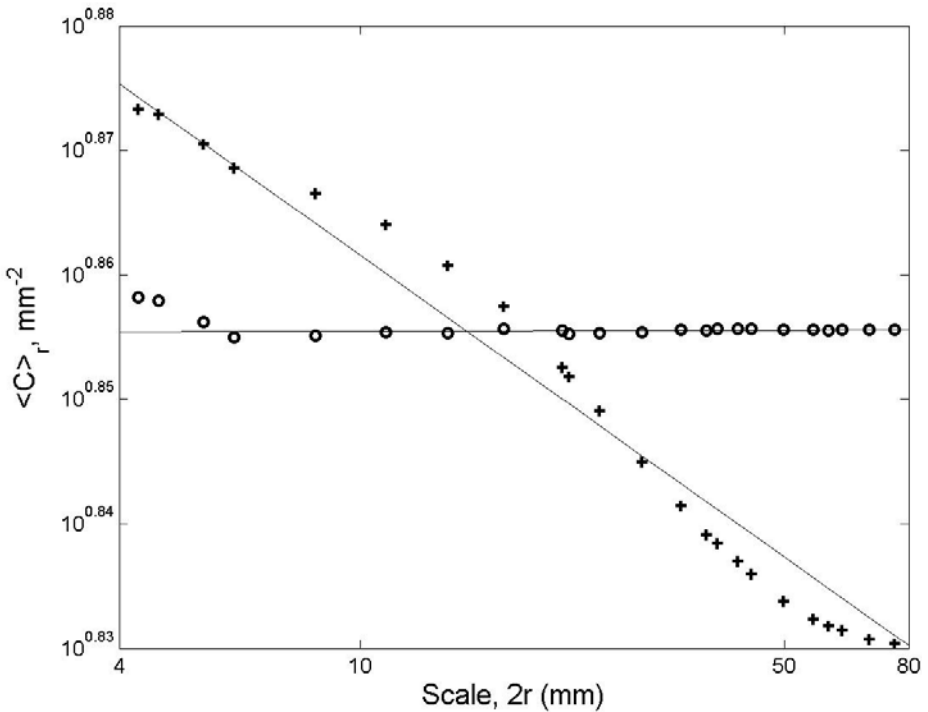


Figure 8. The details of the dependence of local droplet concentration $\langle C \rangle_r$ on scale for the artificially generated Poisson test image (o) and for experimental image number one (+) calculated according to (7). See text for details.

5. DISCUSSION

At this point we can state that the results of the correlation analysis are consistent with those of the classical analysis, in the sense that both indicate a difference between the Poisson distribution of droplets in space and that observed. The adopted correlation analysis gives an intuitive measure of this difference, in terms of the scale dependence of the local droplet concentration.

Fitting straight lines to the data in all ten panels of Fig. 7 gives estimates of the scaling exponent $D - 2$ (according to (8)) for all the investigated images in the range of scales from 4 to 80 mm. Values of these estimates are presented in Table 1. Note that the difference between the estimated correlation dimension of droplet distributions and the Euclidean dimension are small. This, however, still results in non-negligible dependence of the local droplet concentration on scale.

It is worth mentioning that such a small difference between the Euclidean dimension and the scaling exponent can be observed in Figs. 4 and 5 of Malinowski *et al.* (1994), where high-resolution FSSP data from the Hawaiian clouds are presented. In that paper the deviations from the Euclidean dimension were interpreted as unimportant; the re-interpretation of the data in terms of local droplet concentration shows that that conclusion was not correct.

While shapes of curves plotted in Figs. 5–7 are similar for all the experimental images, there are noticeable differences in their quantitative characteristics. These are not directly related to the droplet density (Table 1), and probably reveal real differences in the particular realizations of the turbulent flow in the plane of the image at the moment of imaging. This is verified by the visual inspection of the consecutive images; visible

patterns clearly differ from case to case. Remember that we observe a small and compact volume of the flow, with only a few small-scale turbulent eddies. In such an approach this kind of variability is inevitable.

The most stunning result of the experiment is that even weak turbulence causes clustering of droplets, which are characterized by a small Stokes number. Note, that this is in agreement with the theoretical work of Falkovich and Pumir (2004), who performed a series of numerical simulations of particles in turbulent flow in conditions close to those in our chamber. In their experiments the smallest Stokes number was 0.02 which is not far from our values of 0.006–0.012, and their Re_λ varied from 21 to 130 whilst our estimated value is 80 which is near the middle of this range. They argue, that for Re_λ of the order of 100, even for a Stokes number as small as 0.02, the second order statistics of droplet concentration are still affected by turbulence. Additionally they show that gravitational settling may enhance droplet clustering, where for $S \leq 0.02$ (S is a nondimensional number characterizing the importance of gravitational settling of droplets with respect to turbulent motions) the droplet concentration fluctuations are insensitive to the turbulence intermittency (i.e. to Re_λ). S depends on the Stokes number, Kolmogorov velocity-scale and the terminal velocity, and takes the form:

$$S = \varepsilon^{3/4} / g\nu^{1/4}, \quad (10)$$

where g is the gravitational acceleration and ν is the air viscosity. Note, that S is independent of droplet size. The value of S in the chamber, equal to 0.0011, is in agreement with this condition. It has to be emphasised that Grabowski and Vaillancourt (1999), using the same nondimensional characteristics, argued that gravitational sedimentation should be accounted for when investigating droplet clustering in weak turbulence. This argument now has theoretical and experimental support.

6. CONCLUSIONS

Positions of cloud droplets were observed in a weakly turbulent environment inside a cloud chamber by means of laser sheet photography. Those positions were analysed with simple tests verifying the assumption of the Poisson distribution character of droplet spacing, and also by means of correlation analysis. The results obtained by both methods reveal deviations from the random distribution of droplets in space, but do not clearly indicate any preferred scale at which the droplet concentration is increased. It must be emphasized that our results are statistically significant, as we were able to observe a large number of droplets in relatively uniform conditions. At least 200 000 droplets were detected in each image.

A comparison of Figs. 5 and 6 reveals differences in the interpretation of the droplet distribution data in terms of (2) and (3). At a first glance, Fig. 4 could be interpreted in such a way that the deviations from the Poisson distribution (reference image) are important at scales above 8 mm. Figure 6, which can be interpreted as a planar density of clustering index presented in Fig. 5, gives a different impression—the deviations from the Poisson distribution are noticeable in the whole range of investigated scales, with the maximum deviation around 3–4 mm. Additionally, the importance of this deviation from the random distribution is uncertain. A similar problem can be seen in Figs. 1–4 in Chaumat and Brenguier (2001). The authors compare experimental droplet distributions to the corresponding Poisson distributions and analyse them with a Fishing test (Baker 1992), which is a variant of (2) and (3). The deviations from the Poisson distribution can be seen, but they can be interpreted either as noticeable or as unimportant depending on

the adopted method of presentation (clustering index, Fishing test, volume averaged pair correlation function) and the selected level of confidence.

In order to look at the problem from a different perspective, we propose a correlation analysis in terms of (7). The local concentration $\langle C \rangle_r$, defined by (6) and (7), gives a different view of the problem of droplet spacing. When investigating whether the droplet distribution is random ((2), (3), Fishing test) a change from volume averaging to local averaging performed with the correlation analysis (4)–(8) clearly reveals the clustering of droplets at small scales. The 3–10% decrease in the local droplet concentration in the range of scales between 4 and 80 μm , observed in all the images, gives an intuitive idea of the importance of this effect in weak turbulence in the cloud chamber, that is to say in turbulence less vigorous and less intermittent than in most clouds. The small differences between the scaling exponent estimated according to (5) and the Euclidean dimension $E = 2$, indicate that, at least in the chamber, the distribution of droplets is close to ‘space-filling random’. Nevertheless, even this small deviation from space-filling yields a noticeable effect on the local droplet concentration, representing the neighbourhood of an average droplet.

In typical cloud measurements the mean droplet concentration is estimated by volume averaging the counts from the FSSP probe. The comparison of $\langle C \rangle_r$ and the mean droplet concentration in the whole image (which can be regarded as a surrogate of the typical data from the *in situ* measurements) presented in Fig. 8 shows noticeable differences between them. The conclusion is that a typical cloud droplet may have more close neighbours than expected from the mean droplet concentration in the volume. This, however, has to be verified by applying the correlation analysis to data from *in situ* measurements in real clouds.

ACKNOWLEDGEMENTS

This research was supported by grants 6 P04D 038 20 and 5 T07A 052 24 from the Polish State Committee for Scientific Research (KBN). We also thank Dr J. L. Brenguier, Dr W. W. Grabowski and anonymous reviewers for their comments and suggestions.

REFERENCES

- Andrejczuk, M., Grabowski, W. W., 2004 Numerical simulation of cloud–clear air interfacial mixing. *J. Atmos. Sci.*, **61**, 1726–1739
- Malinowski, S. P. and Smolarkiewicz, P. K. 2000 ‘Influence of a small-scale turbulence structure on the concentration of cloud droplets’. Pp. 159–162 in Volume I of Proceedings of the 13th international conference on clouds and precipitation, Reno, Nevada 14–18 August 2000. International Commission on Clouds and Precipitation of the International Association of Meteorology and Atmospheric Sciences
- Bajer, K., Malinowski, S. P. and Markowicz, K. 2000
- Baker, B. A. 1992 Turbulent entrainment and mixing in clouds: A new observational approach. *J. Atmos. Sci.*, **49**, 387–404
- Baumgardner, D., Weaver, K. and Baker, B. 1993 A technique for the measurement of cloud structure on centimeter scales. *J. Atmos. Oceanic Technol.*, **10**, 557–563
- Brenguier, J. L. 1993 Observation of cloud structure at the centimeter scale. *J. Appl. Meteorol.*, **32**, 783–793
- Chamat, L. and Brenguier, J. L. 2001 Droplet spectra broadening in cumulus clouds. Part II: Microscale droplet concentration heterogeneities. *J. Atmos. Sci.*, **58**, 642–654
- Falconer, K. 1990 *Fractal geometry: Mathematical foundations and applications*. John Wiley and Sons, New York, USA
- Falkovich, G. and Pumir, A. 2004 Intermittent distribution of heavy particles in a turbulent flow. *Phys. Fluids*, **16**, L47–L50

- Feder, J. 1988 *Fractals*. Plenum Press, New York, USA
- Grabowski, W. W. and Vaillancourt, P. 1999 Comments on preferential concentration of cloud droplets by turbulence: Effects on the early evolution of cumulus cloud droplet spectra. *J. Atmos. Sci.*, **56**, 1433–1441
- Jeffery, C. A. 2001 Investigating the small-scale structure of clouds using the delta-correlated closure: Effect of particle inertia, condensation/evaporation and intermittency. *Atmos. Res.*, **59–60**, 199–215
- Jonas, P. R. 1996 Turbulence and cloud microphysics. *Atmos. Res.*, **40**, 283–306
- Kostinski, A. B. 2001 On the extinction of radiation by a homogeneous but spatially correlated random medium. *J. Opt. Soc. Am. A.*, **18**, 1929–1933
- Kostinski, A. B. and Shaw, R. A. 2001 Scale-dependent droplet clustering in turbulent clouds. *J. Fluid Mech.*, **434**, 389–398
- Kozikowska, A., Haman, K. and Supronowicz, J. 1984 Preliminary results of an investigation of the spatial distribution of fog droplets by a holographic method. *Q. J. R. Meteorol. Soc.*, **110**, 65–73
- Landau, L. D. and Lifshitz, E. M. 1980 *Statistical physics*. Butterworth Heinemann, Oxford, UK. (In Polish: 1959 *Fizyka statystyczna*. PWN, Warsaw, Poland)
- Malinowski, S. P. and Jaczewski, A. 1999 Laboratory investigation of the droplet concentration at the cloud-clear air interface. *Phys. Chem. Earth*, **24**, 477–480
- Malinowski, S. P., Leclerc, M. Y. and Baumgardner, D. G. 1994 Fractal analyses of high resolution cloud droplet measurements. *J. Atmos. Sci.*, **51**, 397–413
- Malinowski, S. P., Zawadzki, I. and Banat, P. 1998 Laboratory observations of cloud-clear air mixing at small scales. *J. Atmos. Oceanic Technol.*, **15**, 1060–1065
- Meakin, P. 1998 *Fractals, scaling and growth far from equilibrium*. Cambridge University Press, Cambridge, UK
- Pawlowska, H., Brenguier, J. L. and Salut, G. 1997 Optimal nonlinear estimation for cloud particle measurements. *J. Atmos. Oceanic Technol.*, **14**, 88–104
- Pinsky, M. and Khain, A. 2001 Fine structure of droplet concentration as seen from the Fast-FSSP measurements: Methods of analysis and preliminary results. *J. Appl. Meteorol.*, **40**, 1515–1537
- 2003 Fine structure of droplet concentration as seen from the Fast-FSSP measurements. Part II: Results of *in situ* observations. *J. Appl. Meteorol.*, **42**, 65–73
- Shaw, R. A. 2003 Particle-turbulence interactions in atmospheric clouds. *Ann. Rev. Fluid Mech.*, **35**, 183–227
- Shaw, R. A., Reade, W. C., Collins, L. R. and Verlinde, J. 1998 Preferential concentration of cloud droplets by turbulence: Effects on the early evolution of cumulus cloud droplet spectra. *J. Atmos. Sci.*, **55**, 1965–1976
- Shaw, R. A., Kostinski, A. B. and Larsen, M. L. 2002 Towards quantifying droplet clustering in clouds. *Q. J. R. Meteorol. Soc.*, **128**, 1043–1057
- Sreenivasan, K. R. and Antonia, R. A. 1997 The phenomenology of small-scale turbulence. *Ann. Rev. Fluid Mech.*, **29**, 435–472
- Uhlig, E. M., Borrmann, S. and Jaenicke, R. 1998 Holographic *in-situ* measurements of the spatial droplet distribution in stratiform clouds. *Tellus B*, **50**, 377–387
- Vaillancourt, P. A. and Yau, M. K. 2000 Review of particle-turbulence interactions and consequences for cloud physics. *Bull. Am. Meteorol. Soc.*, **81**, 285–298
- Vaillancourt, P. A., Yau, M. K., Bartello, P. and Grabowski, W. W. 2002 Microscopic approach to cloud droplet growth by condensation. Part II: Turbulence, clustering and condensational growth. *J. Atmos. Sci.*, **59**, 3421–3435